Harnessing the Power of Adiabatic Curve Crossing to Populate the Highly Vibrationally Excited H_2 ($v = 7, j = 0$) Level

William E. Perreault, Haowen Zhou, Nandini Mukherjee,* and Richard N. Zare†
Department of Chemistry, Stanford University, Stanford, California 94305, USA

(Received 29 January 2020; accepted 30 March 2020; published 24 April 2020)

A large ensemble of $\sim 10^9$ H_2 ($v = 7$, $j = 0$) molecules is prepared in the collision-free environment of a supersonic beam by transferring nearly the entire H_2 ($v = 0$, $j = 0$) ground-state population, where v and j are the vibrational and rotational quantum numbers, respectively. This is accomplished by controlling the crossing of the optically dressed adiabatic states using a pair of phase coherent laser pulses. The preparation of highly vibrationally excited H_2 molecules opens new opportunities to test fundamental physical principles using two loosely bound yet entangled H atoms.

DOI: 10.1103/PhysRevLett.124.163202

Highly vibrationally excited diatomic molecules are intrinsically interesting quantum systems with two increasingly loosely bound yet nonetheless entangled atoms [1,2]. There is a longstanding interest to produce such highly delocalized systems, which have many useful applications from testing fundamental principles of quantum physics [3] to studying cold chemical reactions with a pair of nearly dissociated atoms [4–7]. Full understanding of quantum phenomena, such as tunneling resonances, is only possible when we eliminate macroscopic averaging by selecting a single rovibrational quantum state. Here we describe the optical preparation of a highly vibrationally excited single quantum state of the hydrogen molecule.

Theoretical studies show that high vibrational excitation in H_2 molecules plays an important role in overcoming the activation barriers of cold chemical reactions, including those in interstellar gas clouds [8–10]. This work leads us to question at what level of vibrational stretch do the atoms in a H_2 molecule become reactive in a collision with another partner? Prior experimental [11] and theoretical [12,13] work on the controversial four center reaction $H_2 + D_2 \rightarrow 2\ HD$ indicates that the 7th vibrationally excited level of H_2 may be energetic enough to overcome the activation barrier. Preparation of this level would allow us to experimentally study the quantum dynamics of this reaction at low collision energies. Additionally, high-lying vibrational levels of H_2 are considered essential to the efficient generation of H^- beams by dissociative attachment of electrons, which has important applications in fusion devices [14,15].

In spite of longstanding interest, it remains difficult to optically prepare highly vibrationally excited quantum states of fundamental molecules like H_2. This is because of the reduced overlap (small Franck-Condon factor) between the ground and excited vibrational wave functions. In molecules with optically accessible intermediate resonances, stimulated Raman adiabatic passage (STIRAP) [16–18], among other coherent techniques [19,20], has been shown to achieve population transfer to highly vibrationally excited states [21–23]. However, molecules with widely separated electronic states such as H_2, N_2, HCl, and CO require an excitation technique that does not make use of a resonant intermediate state. In these systems, two-photon excitation becomes inefficient with increasing vibrational quantum number of the target state [24–27] to the point that it appears nearly impossible to transfer any population directly to high vibrational states. Is it possible to use intense laser fields to compensate for the weak two-photon coupling, while simultaneously creating an avoided crossing of the optically dressed states that will transfer population to a highly vibrationally excited state? In this work, we explore this question through our effort to produce a high concentration of H_2 molecules in the seventh vibrational level, which has never before been achieved.

The technique employed in this work to control the crossing of adiabatic states is known as Stark-induced adiabatic Raman passage (SARP) [27]. SARP manipulates the adiabatic crossings using the Stark shift induced by a pair of phase coherent laser pulses. The efficiency of adiabatic population transfer relies on a slow sweeping rate of the Stark-induced detuning and a strong two-photon Rabi frequency to lift the degeneracy of the adiabatic states at the crossing [26,28]. The two-photon H_2 $(v = 0, j = 0) \rightarrow (v = 7, j = 0)$ transition studied here has a very weak Rabi frequency accompanied by a large dynamic Stark shift. Here, v and j refer to the vibrational and rotational quantum numbers, respectively. In contrast to our earlier work on SARP populating lower v states [28–30], the unfavorable material parameters in this transition create completely different crossing dynamics of the adiabatic potentials that challenge SARP population

transfer. By carefully tuning the optical field parameters, we demonstrate complete population transfer to the $(v = 7)$ vibrational level. The case of a very weakly coupled two-photon system gives us the opportunity to examine experimentally the subtle character of adiabatic curve crossing and its critical dependence on the external fields in unprecedented depth. We thus present an instructive model system that elucidates the fundamental dynamics of adiabatic curve crossings. Similar curve crossing dynamics play a major role in systems ranging from coherent optical interactions [31,32] to collision dynamics [33].

The adiabatic eigenstates of the optically dressed Hamiltonian are expressed as follows: $|+\rangle = \sin\theta|1\rangle + \cos\theta|2\rangle$ and $|-\rangle = \cos\theta|1\rangle - \sin\theta|2\rangle$, where $|1\rangle$ and $|2\rangle$ refer to the initial and the final bare states, respectively. The mixing angle θ is defined by $\cos\theta = \sqrt{(\tilde{\Omega} + \Delta)/2\tilde{\Omega}}$ and $\sin\theta = \sqrt{(\tilde{\Omega} - \Delta)/2\tilde{\Omega}}$ where $\tilde{\Omega} = \sqrt{\Delta^2 + 4\Omega_R^2}$ [34]. Here, Ω_R is the two-photon Rabi frequency, and Δ is the dynamic Stark-induced two-photon detuning. The crossing of the adiabatic states with energies $E_\pm = \pm\tilde{\Omega}/2$ is avoided at resonance when the two-photon Rabi frequency Ω_R is nonzero. As Δ sweeps through resonance $(\Delta = 0)$ from a large positive to a large negative value, the adiabatic eigenstate $|-\rangle$, which initially coincides with the ground state $|1\rangle$, rotates by 90°, aligning parallel to the target state $|2\rangle$ at the end of excitation [28]. To transfer population, the adiabatic states must remain decoupled throughout the excitation process so that the population remains trapped within $|-\rangle$. This condition requires a slow rotation of the adiabatic states defined by [28,34–36]

$$d\theta/dt \ll |E_\pm|. \tag{1}$$

Large scanning rates $d\theta/dt$ will introduce nonadiabatic transitions between the adiabatic states causing Rabi oscillations and inconsistent population transfer. At resonance, Eq. (1) reduces to $d\Delta/dt \ll 4\Omega_R^2$, which shows that SARP requires a minimum Rabi frequency to create a strongly avoided crossing that prevents mixing of the adiabatic states [28].

Figure 1 shows the temporal dynamics of SARP population transfer from $H_2\,(v = 0, j = 0) \rightarrow (v = 7, j = 0)$, using a sequence of a strong pump pulse followed by a weaker Stokes pulse. This pulse sequence creates two resonance crossings: an entirely unavoided $(\Omega_R = 0)$ first crossing and a strongly avoided second crossing where near complete population transfer occurs [28]. The numerical simulation in Fig. 1 suggests that a strongly avoided crossing can be achieved even with weak two-photon coupling and large Stark shift such that the population remains almost completely trapped within one of the adiabatic states.

The two-photon Rabi frequency (Ω_R) and Stark-induced detuning (Δ) that control the condition of adiabatic curve

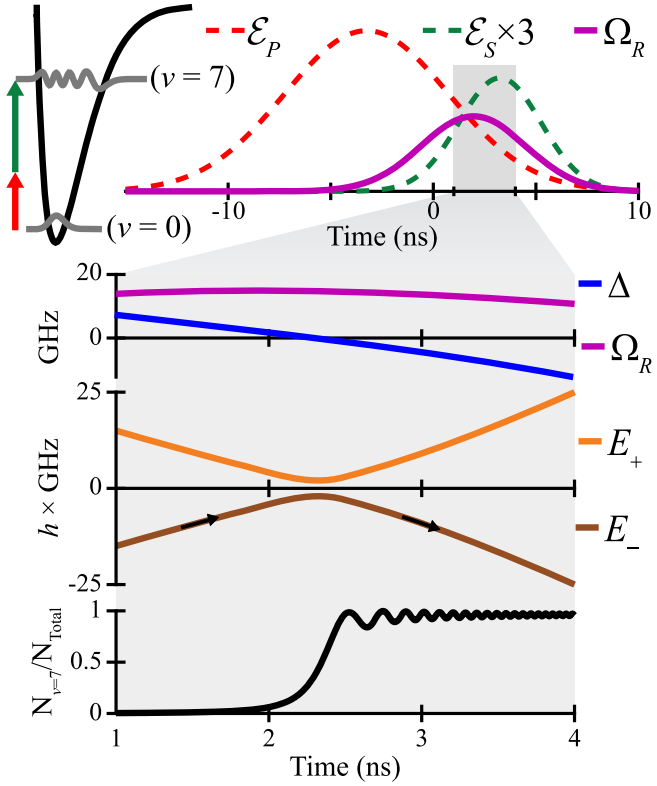

FIG. 1. Two-photon Stark-induced adiabatic Raman passage transferring population from $H_2\,(v = 0) \rightarrow (v = 7)$. The calculation solves the time-dependent Schrödinger equation using a Gaussian temporal profile for the pump $\mathcal{E}_P$ (red dashed) and weaker Stokes $\mathcal{E}_S$ (green dashed) optical fields with $1/e$ width of 8 and 4 ns, respectively. The overlap region of the pump and Stokes is expanded to illustrate the two-photon Rabi frequency Ω_R (purple solid line), the dynamic Stark shift Δ (blue), the adiabatic energies E_+ (orange) and E_- (brown), and fractional population transfer (black) at the avoided crossing. The black arrows on the E_- curve indicate that population is carried via the adiabatic state $|-\rangle$. The inset showing the wave functions for the involved vibrational state was adapted from a prior publication [24].

crossing in Eq. (1) are produced by the optical fields. $\Omega_R = r_{0v}\mathcal{E}_P\mathcal{E}_S/\hbar$ and $\Delta = \Delta_0 - \alpha_{0v}(|\mathcal{E}_P|^2 + |\mathcal{E}_S|^2)/\hbar$ [27], where, $\mathcal{E}_P$ and $\mathcal{E}_S$ give the time-dependent optical field amplitudes of the pump and Stokes pulses, respectively. For the $0 \rightarrow v$ transition, r_{0v} is the Raman coupling [37], and α_{0v} is the difference optical polarizability defined by $\alpha_{0v} = \alpha(v) - \alpha(v = 0)$. Δ_0 is the field-free detuning. The $H_2\,(v = 0, j = 0) \rightarrow (v = 7, j = 0)$ transition pushes these material parameters to their limiting values [28] with r_{07} only ~4% of r_{01}, while α_{07} is ~15 times larger than α_{01} [27,37]. The decreasing of r_{0v} and simultaneous increasing of α_{0v} with increasing vibrational quantum number v of the target state makes it increasingly difficult to achieve a strongly avoided crossing, promoting nonadiabatic transitions. We chose the $(j = 0) \rightarrow (j = 0)$ transition to minimize α_{07}, thus reducing the Stark shift. In the remainder of

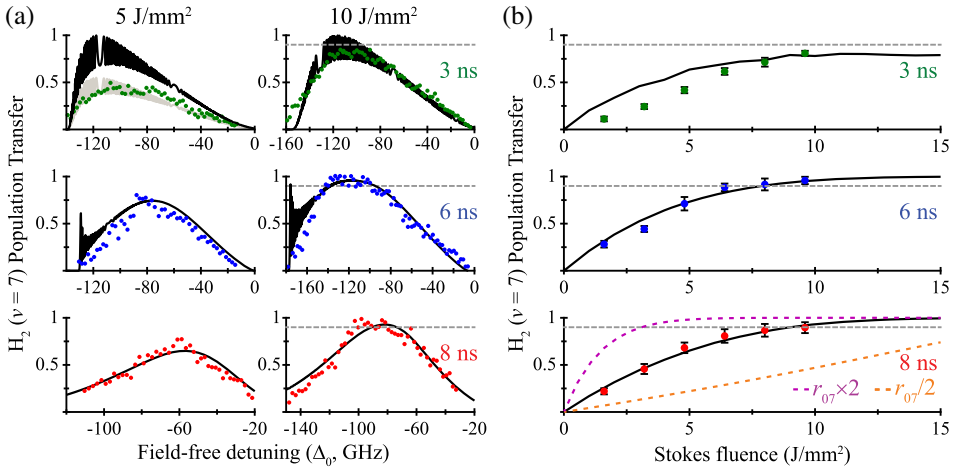

FIG. 2. Comparison of our experimental data and theoretical calculations for the H_2 $(v = 0) \rightarrow (v = 7)$ transition. The dots show scaled experimental data for three delays: 3 (green), 6 (blue), and 8 ns (red). See text for a description of how the REMPI signal is scaled to represent the population transfer. The solid black curves show corresponding simulations, as in Fig. 1 with an 8 ns Gaussian pump pulse, a 4 ns Gaussian Stokes pulse, and a fixed pump fluence of 100 J/mm^2. (a) SARP spectra at Stokes fluences of 5 and 10 J/mm^2. Each experimental data point is found by averaging the H_2 $(v = 7)$ REMPI signal over 128 laser pulses. The gray dashed lines for the 10 J/mm^2 plots show 90% transfer. The light gray curve in the 3 ns 5 J/mm^2 plot was obtained by scaling down the theoretical curve to illustrate that the shape of the experimental spectrum is reproduced. (b) SARP saturation as a function of the Stokes fluence. Each experimental data point is determined by averaging over the peak of the SARP spectrum at the given Stokes fluence. For the 8 ns delay, we show two additional theoretical curves calculated by setting the Raman coupling to twice (purple dashed) and half (orange dashed) of the value used to generate the black curves.

the Letter, we omit the rotational quantum number for brevity.

The SARP experimental setup has been detailed elsewhere [28]. Briefly, following an optical delay line, a Stokes pulse (671 nm, ~10 J/mm^2) is combined with a stronger pump pulse (1064 nm, 100 J/mm^2). The two SARP pulses are then focused on to a skimmed supersonically expanded beam of H_2 molecules. The vibrationally excited H_2 $(v = 7, j = 0)$ molecules are detected state-selectively using $(2 + 1)$ resonance enhanced multiphoton ionization (REMPI) through the $(v' = 6, j' = 0)$ level of the $E,F\ ^1\Sigma_g^+$ electronic state with a VUV pulse at 252.297 nm (vac). The $(2 + 1)$ REMPI signal is directly proportional to the population transfer to the $(v = 7)$ level. The population transfer is determined by comparing the experimentally measured REMPI signal as a function of laser fluence and frequency with theory [28].

We measure the H_2 $(v = 7)$ REMPI signal as the two-photon field-free detuning is scanned for fixed pump and Stokes fluences. The field-free detuning is defined as $\Delta_0 = \omega_P + \omega_S - \omega_{70}$, where ω_P and ω_S are the frequencies of the pump and Stokes optical fields, and ω_{70} is the frequency for $(v = 0) \rightarrow (v = 7)$ transition in the absence of light. We measure ω_{70} to be 728.129 THz, which agrees with a previously calculated value [38] within ~4 GHz. From the REMPI signal as a function of field-free detuning, which we will refer to as the SARP spectrum, we are able to quantify the Stark shift and extract the two important material parameters r_{07} and α_{07}.

We collected a series of SARP spectra for six different Stokes fluences from 2 to 10 J/mm^2 and three different pump-to-Stokes delays, while the pump fluence was kept fixed at 100 J/mm^2. Figure 2(a) shows the SARP spectra for two specific Stokes fluences of 5 and 10 J/mm^2 at pump-to-Stokes delays of 3, 6, and 8 ns. The negative detuning shows that the two-photon transition is redshifted, mainly by the intensity of the stronger 1064 nm pulse. The large magnitude of the Stark shift is caused by the large polarizability of the $(v = 7)$ level. The solid curve in each plot represents the theoretically calculated population transfer, which is determined by solving the time-dependent Schrödinger equation as in Fig. 1 for each detuning. The laser fluences have been estimated using a beam camera that was carefully positioned to reflect the laser beam sizes on the molecular beam.

The values for r_{07} and α_{07} were found by maximizing the correspondence between the theoretically calculated and experimentally measured SARP spectra for all six Stokes fluences for the delay of 8 ns. We find the two-photon coupling coefficient $r_{07} = 0.13 \times 10^{-41}$ Cm/(V/m) and the difference polarizability $\alpha_{07} = 5.3 \times 10^{-41}$ Cm/(V/m). These values were then used to calculate the theoretical SARP spectra shown by the black curves in Fig. 2(a). The 6 ns delay in Fig. 2(a) also shows good agreement between theory and experiment, confirming that we have obtained the correct values of the material parameters. The theoretical 6 ns SARP spectrum in Fig. 2(a) shows population oscillations for large field-free detuning. These oscillations are

caused by nonadiabatic coupling at multiple partially avoided crossings, and should not be confused with the temporal oscillations shown in Fig. 1. These oscillations are even stronger for the 3 ns delay, but nonetheless the theoretically calculated SARP spectrum matches fairly well with experiment for 10 J/mm^2. The shape of the spectrum at 5 J/mm^2 also matches, but a significant discrepancy is observed in the magnitude of the population transfer. This discrepancy results from the strong nonadiabatic coupling, which causes population transfer to be sensitive to laser intensity fluctuations.

To explain the population oscillations present in the 3 and 6 ns SARP spectra, we discuss the dynamics of adiabatic curve crossing. SARP population transfer is maximized when the field-free detuning is set such that the Rabi frequency maximizes at one of the two resonance crossings, while it becomes negligible at the other crossing. A weakly avoided first crossing will initiate rapid Rabi oscillations, which prevent population transfer via a single adiabatic state at the second, strongly avoided crossing. Because these Rabi oscillations are highly sensitive to the field-free detuning and laser fluence, the population transfer can vary wildly with small changes in laser parameters. For the 6 ns delay at large detuning, the first crossing becomes very weakly avoided, creating small population oscillations. In contrast, for 3 ns delay the first resonance crossing is weakly avoided for all field-free detunings, explaining the strength and breadth of the fluctuations for the 3 ns spectrum.

Figure 2(b) shows the experimentally measured H_2 $(v = 7)$ REMPI signal as a function of the Stokes fluence for the three different inter-pulse delays. Each experimental data point represents the maximum population transfer for a given Stokes fluence. The solid curve shows the results of theoretical simulations using the values of r_{07} and α_{07} found earlier. Because of our choice of a strong pump pulse and a much weaker Stokes pulse, the adiabatic condition given in Eq. (1) approximately reduces to a threshold condition for the intensity or fluence of the weaker Stokes pulse [28]. Thus, a successful adiabatic passage manifests itself as the saturation against Stokes pulse fluence seen in both theory and experiment in Fig. 2(b). The saturation behavior at high Stokes fluences allows us to determine a scale factor to convert the REMPI signal to experimental population transfer for each delay [28].

Figure 2(b) shows exceptional agreement between theory and experiment for both the 6 and 8 ns delays. For the 8 ns delay, we show two additional theoretical curves calculated by varying the Raman coupling. Clearly, the experimental data does not match with either of these two curves, providing further evidence that we have extracted the correct value for the Raman coupling. For the 8 ns delay our measurement shows ~90% transfer using the maximum Stokes fluence of 10 J/mm^2 available in our experiment. For the 6 ns delay saturation is reached at a slightly lower Stokes fluence, achieving > 90% transfer at the Stokes fluence of 10 J/mm^2. As we will demonstrate below, Eq. (1) is best satisfied for the 6 ns delay, so the crossing of the adiabatic energies is avoided with a large margin (see Fig. 3) enabling SARP to achieve near complete population transfer. Figure 2(b) shows that with a Stokes fluence >13 J/mm^2 it is possible to achieve near complete population transfer for both 6 and 8 ns delays.

In contrast, for the 3 ns delay, Fig. 2(b) shows some discrepancy between theory and experiment but the overall trend is in reasonable agreement. The nonadiabatic interactions at multiple avoided crossings for the 3 ns delay make the population transfer highly sensitive to the laser fluence. We thus attribute the discrepancy between theory and experiment in the 3 ns case to laser pulse-to-pulse energy fluctuations, which are not included in our theory. The ability to ignore these pulse-to-pulse fluctuations at larger delays is one of the most useful features of SARP as an experimental tool.

Figure 3 examines the avoided crossing condition in Eq. (1) by comparing the nonadiabatic coupling $d\theta/dt$ with the adiabatic energy at three different interpulse delays. For each delay the temporal evolution is calculated using the

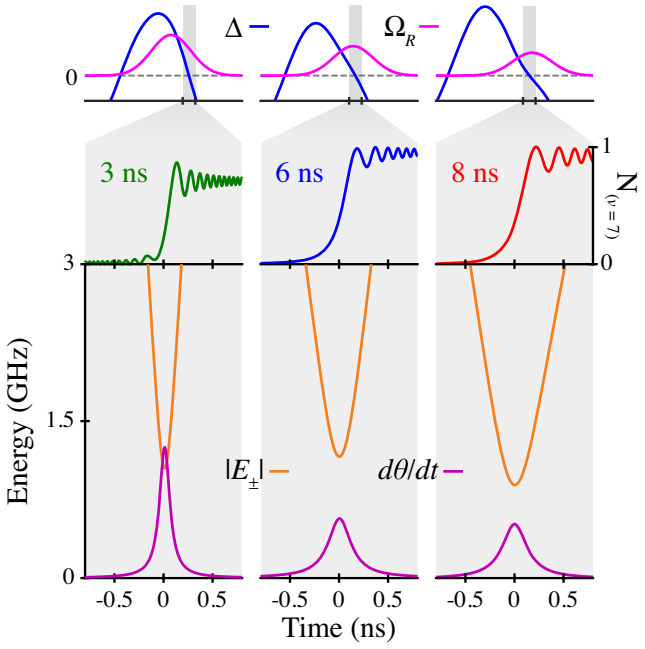

FIG. 3. The adiabatic condition near the zero crossing of the Stark-induced detuning for the three pump-to-Stokes delays. For each delay the nonadiabatic coupling $d\theta/dt$ (purple curve) is compared with the adiabatic energy $|E_\pm|$ (yellow curve). The corresponding Rabi frequency (Ω_R, top), detuning (Δ, top), and population transfer (center) are shown for each delay. These curves were calculated using a field-free detuning that corresponds to the peak of the SARP spectrum [Fig. 2(a)] for the maximum Stokes fluence of 10 J/mm^2. For 3 ns, the adiabatic condition $d\theta/dt < |E_\pm|$ is not satisfied, explaining the incomplete population transfer shown.

field-free detuning that corresponds to the peak of the SARP spectrum shown in Fig. 2(a) at 10 J/mm^2 Stokes fluence. The top panel shows how the adiabatic condition is influenced by $d\Delta/dt$ and Ω_R. Figure 3 shows that the adiabatic following condition, $d\theta/dt < |E_\pm|$, is best satisfied for the 6 ns delay, as the Rabi frequency is maximized at $\Delta = 0$ achieving >90% population transfer via nearly perfect adiabatic passage. Although the peak of the Rabi frequency also aligns with the crossing for the 8 ns delay, the adiabatic condition is not as strongly satisfied. Theory shows that at higher Stokes fluence the crossing is more strongly avoided and complete population transfer can be achieved.

As mentioned earlier, there are two partially avoided crossings for the 3 ns delay for any field-free detuning, which prevent complete population transfer. In Fig. 3, the detuning is chosen to minimize the strength of the first crossing, although it is still weakly avoided (top panel) as revealed by the small Rabi oscillations shown by the green curve at −0.5 ns. The second crossing is not strongly avoided because $d\Delta/dt$ is large and Ω_R does not maximize at resonance. This results in mixing of the adiabatic states and incomplete population transfer. For larger values of the field-free detuning, one of the crossings can be made strongly avoided. However, the population transfer is nonetheless limited because the Rabi frequency at the other crossing is non-negligible, which either initiates mixing of the adiabatic states destroying the condition for ideal adiabatic passage, or causes partial coherent population return. This explains the saturation at 80% population transfer.

The fact that SARP population transfer to H_2 $(v = 7)$ requires a relatively large interpulse delay is counterintuitive because the weaker two-photon coupling would seem to demand stronger overlap between the pump and Stokes pulses. However, our examination of the 3 ns dynamics demonstrates that multiple partially avoided crossings limit population transfer at shorter delays. At larger delays it is possible to create a single strongly avoided crossing for a wide range of initial detunings and Stokes fluences, achieving complete population transfer that is insensitive to intensity and frequency fluctuations (see Supplemental Material [39]).

Close comparison of experimental saturation data with theory allowed us to determine the fractional population transfer, from which we estimate that we have produced ~10^9 H_2 $(v = 7, j = 0)$ molecules. Our ability to stably produce such large concentrations of H_2 molecules in the $(v = 7, j = 0)$ rovibrational level will not only allow us to probe the much debated four-center reactions, we will also be able to experimentally verify the theoretically predicted rate of vibrational cooling in cold interstellar gas clouds [5]. Additionally, our success in generating the $(v = 7, j = 0)$ state, in conjunction with our theoretically developed multistep SARP process [25], shows that SARP has the ability to prepare any H_2 vibrational level. Production of highly vibrationally excited levels of H_2, which should increasingly act as a dissociated pair of H atoms, open new possibilities to study long-range interactions that are important throughout physics and chemistry.

This work has been supported by the U.S. Army Research Office under ARO Grants No. W911NF-19-1-0163 and No. W911NF-19-1-0283.

*Corresponding author.
nmukherj@stanford.edu
†Corresponding author.
zare@stanford.edu

[1] L. P. H. Schmidt *et al.*, Spatial Imaging of the H_2^+ Vibrational Wave Function at the Quantum Limit, Phys. Rev. Lett. **108**, 2 (2012).
[2] D. Akoury *et al.*, The simplest double slit: Interference and entanglement in double photoionziation of H_2, Science **318**, 949 (2007).
[3] B. K. Kendrick, J. Hazra, and N. Balakrishnan, Geometric Phase Appears in the Ultracold Hydrogen Exchange Reaction. Phys. Rev. Lett. **115**, 153201 (2015).
[4] N. Balakrishnan, R. Forrey, and A. Dalgarno, Threshold phenomena in ultracold atom–molecule collisions, Chem. Phys. Lett. **280**, 1 (1997).
[5] N. Balakrishnan, R. C. Forrey, and A. Dalgarno, Quenching of H_2 Vibrations in Ultracold ^{3}He and ^{4}He Collisions, Phys. Rev. Lett. **80**, 3224 (1998).
[6] H. Hou *et al.*, Enhanced reactivity of highly vibrationally excited molecules on metal surfaces, Science **284**, 1647 (1999).
[7] M. Silva, R. Jongma, R. W. Field, and A. M. Wodtke, The dynamics of stretched molecules: Experimental studies of highly vibrationally excited molecules with stimulated emission pumping, Annu. Rev. Phys. Chem. **52**, 811 (2001).
[8] R. A. Sultanov and N. Balakrishnan, Oxygen chemistry in the interstellar medium: The effect of vibrational excitation of H_2 in the $O(^3P) + H_2$ reaction, Astrophys. J. **629**, 305 (2005).
[9] M. Agundez, J. Goicoechea, J. Cernicharo, A. Faure, and E. Roueff, The chemistry of vibrationally excited H_2 in the interstellar medium, Astrophys. J. **713**, 662 (2010).
[10] E. Roueff and F. Lique, Molecular excitation in the interstellar medium: Recent advances in collisional, radiative, and chemical processes, Chem. Rev. **113**, 8906 (2013).
[11] S. H. Bauer and E. L. Resler, Vibrational excitation in some four-center transition states, Science **146**, 1045 (1964).
[12] K. Morokuma, L. Pedersen, and M. Karplus, Vibrational vs. translational activation in the H_2, H_2 and H_2, D_2 exchange reactions, J. Am. Chem. Soc. **89**, 5064 (1967).
[13] N. J. Brown and D. M. Silver, Comparison of reactive and inelastic scattering of $H_2 + D_2$ using four semiempirical potential energy surfaces, J. Chem. Phys. **72**, 3869 (1980).
[14] I. I. Fabrikant, J. M. Wadhera, and Y. Xu, Resonance processes in e- H_2 collisions: Dissociative attachment and dissociation from vibrationally and rotationally excited states, Phys. Scr. **T96**, 45 (2002).

[15] S. S. Popov, M. G. Atlukhanov, A. V. Burdakov, A. A. Ivanov, A. A. Kasatov, A. V. Kolmogorov, R. V. Vakhrushev, M. Yu. Ushkova, A. Smirnov, and A. Dunaevsky, Neutralization of negative hydrogen and deuterium ion beams using non-resonance adiabatic photon trap, Nucl. Fusion **58**, 096016 (2018).

[16] U. Gaubatz, P. Rudecki, S. Schiemann, and K. Bergmann, Population transfer between molecular vibrational levels by stimulated Raman scattering with partially overlapping laser fields. A new concept and experimental results, J. Chem. Phys. **92**, 5363 (1990).

[17] T. Halfmann and K. Bergmann, Coherent population transfer and dark resonances in SO_2, J. Chem. Phys. **104**, 7068 (1996).

[18] A. Kuhn, S. Steuerwald, and K. Bergmann, Coherent population transfer in NO with pulsed lasers: The consequences of hyperfine structure, Doppler broadening and electromagnetically induced absorption, Eur. Phys. J. D **1**, 57 (1998).

[19] M. M. T. Loy, Two-Photon Adiabatic Inversion, Phys. Rev. Lett. **41**, 473 (1978).

[20] M. Oberst, H. Münch, G. Grigoryan, and T. Halfmann, Stark-chirped rapid adiabatic passage among a three-state molecular system: Experimental and numerical investigations, Phys. Rev. A **78**, 033409 (2008).

[21] E. B. Treacy, Adiabatic inversion with light pulses, Phys. Lett. **27**, 421 (1968).

[22] D. Grischkowsky and M. M. T. Loy, Self-induced adiabatic rapid passage, Phys. Rev. A **12**, 1117 (1975).

[23] N. V. Vitanov, T. Halfmann, B. W. Shore, and K. Bergmann, Laser-induced population transfer by adiabatic passage techniques, Annu. Rev. Phys. Chem. **52**, 763 (2001).

[24] U. Fantz and D. Wunderlich, Franck—Condon factors, transition probabilities and radiative lifetimes for hydrogen molecules and their isotopomeres, At. Data Nucl. Data Tables **92**, 853 (2004).

[25] N. Mukherjee, W. E. Perreault, and R. N. Zare, Stark-induced adiabatic Raman ladder for preparing highly vibrationally excited quantum states of molecular hydrogen, J. Phys. B **50**, 144005 (2017).

[26] N. Mukherjee, W. E. Perreault, and R. N. Zare, Stark-induced adiabatic passage processes to selectively prepare vibrationally excited single and superposition of quantum states, in *Frontiers and Advances in Molecular Spectroscopy* (Elsevier Inc., Cambridge, 2018), pp. 1–46.

[27] N. Mukherjee and R. N. Zare, Stark-induced adiabatic Raman passage for preparing polarized molecules, J. Chem. Phys. **135**, 024201 (2011).

[28] W. E. Perreault, N. Mukherjee, and R. N. Zare, Stark-induced adiabatic Raman passage examined through the preparation of D_2 ($v = 2 j = 0$) and D_2 ($v = 2$, $j = 2$, $m = 0$), J. Chem. Phys. **150**, 234201 (2019).

[29] W. Dong, N. Mukherjee, and R. N. Zare, Optical preparation of H_2 rovibrational levels with almost complete population transfer, J. Chem. Phys. **139**, 074204 (2013).

[30] W. E. Perreault, N. Mukherjee, and R. N. Zare, Preparation of a selected high vibrational energy level of isolated molecules, J. Chem. Phys. **145**, 154203 (2016).

[31] S. L. McCall and E. L. Hahn, Self-Induced Transparency by Pulsed Coherent Light, Phys. Rev. Lett. **18**, 908 (1967).

[32] M. Fleischhauer and M. D. Lukin, Dark-State Polaritons in Electromagnetically Induced Transparency, Phys. Rev. Lett. **84**, 5094 (2000).

[33] J. R. Rubbmark, M. M. Kash, M. G. Littman, and D. Kleppner, Dynamical effects at avoided level crossings: A study of the Landau-Zener effect using Rydberg atoms, Phys. Rev. A **23**, 3107 (1981).

[34] B. W. Shore, The Schrodinger atom, in *The Theory of Coherent Atomic Excitation* (John Wiley & Sons, New York, 1990), pp. 187–262.

[35] L. Landau, Zur Theorie der Energieubertragung. II, Phys. Z. Sowjetunion **2**, 46 (1932).

[36] C. Zener, Non-adiabatic crossing of energy levels, Proc. R. Soc. A **137**, 696 (1932).

[37] S. Chelkowski and A. D. Bandrauk, Raman chirped adiabatic passage: A new method for selective excitation of high vibrational states, J. Raman Spectrosc. **28**, 459 (1997).

[38] J. Komasa, K. Piszczatowski, G. Łach, M. Przybytek, B. Jeziorski, and K. Pachucki, Quantum electrodynamics effects in rovibrational spectra of molecular hydrogen, J. Chem. Theory Comput. **7**, 3105 (2011).

[39] See Supplemental Material at http://link.aps.org/supplemental/10.1103/PhysRevLett.124.163202 for further detail on the experimental method, determination of population transfer, and curve crossing dynamics.